Quantitative Analysis of Single-Electrode Plots to Understand In-Situ Behavior of Individual Electrodes

Journal of The Electrochemical Society, **159** (6) B761-B769 (2012)
0013-4651/2012/159(6)/B761/9/$28.00 © The Electrochemical Society

Quantitative Analysis of Single-Electrode Plots to Understand In-Situ Behavior of Individual Electrodes

Matt S. Naughton, Akash A. Moradia, and Paul J. A. Kenis[z]

Department of Chemical & Biomolecular Engineering, University of Illinois at Urbana-Champaign, Urbana, Illinois 61801, USA

Fuel cells are gaining increasing attention as portable power sources due to their inherent efficiency advantages. Many aspects of electrode and catalyst behavior within an operating fuel cell, however, are still not well-understood. The major divide between catalyst-based rotating disk electrode experiments and full-cell experiments can lead to disappointing results when a promising catalyst is tested in a fuel cell. Here, using a flowing electrolyte-based microfluidic H_2/O_2 fuel cell with a reference electrode, we demonstrate the ability to analyze single-electrode performance in-situ using a novel analysis protocol that provides kinetic parameters R_{ohmic} and $\eta_{kinetic}$ to quantify individual electrode data. Using this protocol, we determine the mass transport and ohmic effects on these kinetic parameters and correlate them with actual fuel cell performance. We also compare the performance of identical electrodes in alkaline and acidic media using both our analytical method and electrochemical impedance. The quantitative parameters are show to predict power density within 5% for measured data and were then used to predict performance for a newly assembled fuel cell, which was accurate within 10% of actual power density inside the measured range. In summary, the analytical method reported here can improve the understanding of in-situ electrode behavior.
 [DOI: 10.1149/2.117206jes]

Manuscript submitted October 24, 2011; revised manuscript received March 5, 2012. Published May 9, 2012.

Fuel cells are especially promising power sources due to their intrinsic advantage of superior efficiency as compared to traditional combustion engines.[1] Research to date has largely been focused on acidic proton exchange membrane (PEM) cells, which use expensive Pt-based catalysts and benefit from well-developed and durable PTFE-based membranes such as Nafion.[1] More recently, research has also focused on solid oxide fuel cells (SOFCs), which can utilize a wide variety of alcohol and hydrocarbon fuels but operate at elevated temperatures (>500°C), making them more suitable for stationary applications.[2–4] Alkaline fuel cells (AFCs) offer a third alternative, with the advantages of superior cathode kinetics and improved catalyst stability.[5–8] Replacement of the expensive Pt-based catalysts with transition metals stabilized in alkaline media could greatly reduce the fuel cell cost, but AFCs are not as well-developed as their acidic counterparts,[5,8] due in part to the incorrect belief that carbon dioxide from air will irreversibly damage AFC electrodes.[7] Each type of fuel cell has its advantages for particular applications, and no single type of fuel cell is likely to become the best option for every application.

One of the major hurdles for fuel cell commercialization is a lack of fundamental understanding of the causes for fuel cell behavior, in particular degradation in performance over time. Fuel cell catalysts are commonly screened using a rotating disk electrode (RDE), which contains a small amount of catalyst (<0.1 mg/cm^2) and is rotated in a dilute solution of electrolyte to control mass transport to the surface.[9,10] This method is designed to isolate the kinetic behavior of various catalysts, but the low loadings and low electrolyte concentrations used in these setups limit the ability to predict catalyst performance in a fuel cell under typical operational conditions. More recently, in a promising method reported by Kucernak et al., gases (i.e. hydrogen or oxygen) are guided over a membrane-mounted electrode, in contrast with the use of dissolved gases in RDE experiments. The use of gaseous reactants allows the system to reach higher current densities than can be obtained with a RDE configuration.[11] While this method better resembles an actual fuel cell, the results are still catalyst-oriented. Some reported conclusions about the superiority of Pt black over Pt/C (in terms of specific activity) would be misleading, given that Pt/C performs better in an actual fuel cell due to the higher surface area on Pt/C despite the higher specific activity of larger Pt particles.[12,13]

Electrochemical half cells have also been used to study fuel cell components, but these half cells suffer from many of the same weaknesses as RDEs. Half cell experiments typically use gases bubbled through solution and a Pt counter electrode.[14,15] While it is possible to test electrodes in these types of setups, the differing method of gas delivery may lead to results that often do not correlate well with results obtained in fuel cell experiments.[16]

Existing methods to characterize *overall* fuel cell performance include measurement of polarization curves, which plot voltage versus current. These curves have three different regions: (i) a kinetic region, in which activation losses dominate the cell behavior; (ii) an ohmic region, in which kinetic, IR, and mass transport losses all have an effect and the polarization curve is roughly linear; and (iii) a mass transport region, where losses from the insufficient supply of reactant(s) cause a significant divergence from the ohmic region of the polarization curve.[17] While polarization curves are highly accurate, they are specific to the fuel cell tested, and much variance in performance occurs due to varying operating conditions. Furthermore, the overall polarization curve does not distinguish between the performance of the different individual electrodes, so identification of the electrode(s) responsible for any identified activation or mass transport losses is difficult. Fuel cell polarization curves can be modeled based on kinetic/ohmic parameters, as has been done previously by, for example, Kim et al. and Yoon et al.,[3,18] but the parameters resulting from these models may be artificial, since they are not based on experimentally measured individual electrode performance.

Electrochemical impedance spectroscopy (EIS) is frequently used to gain deeper understanding of fuel cell behavior. EIS uses an AC current to cause disturbances in the cell which is modeled in a Nyquist analysis as a circuit using a resistor R_{cell}, which indicates the internal cell resistance due to electrolyte and contact resistances, in series with another resistor R_{ct}, the charge transfer resistance due to kinetic losses.[6,17,19] The R_{ct} resistor is in parallel with a capacitor, which represents the double layer capacitance.[6,19] Impedance is a valuable tool for interpreting overall cell performance, but it is specific to a given cell and does not distinguish between different electrodes.

Reference electrodes are a more direct way to understand individual electrode behavior in an operating fuel cell. A reference electrode is used to determine the potential at each electrode, decoupling the effects of anode and cathode behavior. A Ag/AgCl or a saturated calomel electrode is used for a liquid electrolyte fuel cell, while PEM and solid oxide fuel cells typically do not use reference electrodes. A reversible hydrogen electrode (RHE) can be embedded with membranes,[16,20,21] although their accuracy is highly dependent on electrode alignment.[22–25] Anion-exchange membrane fuel cells

[z]E-mail: kenis@illinois.edu

(AEM)[21] and solid oxide fuel cells can also use reference electrodes with the same requirement of proper alignment.[22,25] With even more synthesis, double reference electrodes with a > 0.5 mm electrode offset have been demonstrated to yield IR-corrected potentials within a PEM fuel cell.[26,27] These methods are very powerful ways to provide direct information about electrode performance, although the cumbersome need to fabricate/integrate a reference electrode within non-liquid fuel cells has limited their usage.

Two-electrode plots are typically used to present data obtained with a reference electrode in a fuel cell. Two-electrode plots plot individual electrode potential vs. the reference electrode, and serve as polarization curves for each electrode. These plots are an important way to display single-electrode information, and can be used with liquid electrolyte fuel cells or specially designed membrane fuel cells.[24,28] These plots are also valuable for cathode analysis and can separate out behavior even in cases where both electrodes have significant losses, such as alkaline fuel cells.[6,10,29,30] However, to date these two-electrode plots have been used for largely qualitative analysis based on inward/outward shifts of the polarization curves. They still exhibit the same three qualitative regions found in fuel cell polarization curves (*vide supra*), since the fuel cell polarization curves are just the combination of the polarization curves of the two electrodes.

Here, we report a novel analytical method to quantify individual electrode behavior within an operating fuel cell. This method is based on individual electrode plots in which overpotential is plotted against the equilibrium potential, which is a function of the electrode reaction and the electrolyte pH. These plots are commonly applied in half cell experiments as well as in some full cell experiments.[16,20,31] While in prior work, quantification focused on the kinetic region,[4,32] the ohmic region is the typical range for fuel cell operation and is thus more important for practical applications. To quantify performance of the individual electrodes in a complete cell, we apply a linear fit in the ohmic region, yielding two parameters, R_{ohmic} (the y-axis intercept) and $\eta_{kinetic}$ (the slope). We apply this new approach to demonstrate and quantify the effects of changes in kinetic, ohmic, and mass transport losses within an alkaline fuel cell. The results are then compared to electrode performance in acidic media using both our single-electrode plots obtained in-situ and R_{cell} and R_{ct} values obtained using EIS. Finally, we use the quantitative single-electrode plot results to predict the performance for a newly built fuel cell and compare the predictions with experimental results.

Experimental

Gas diffusion electrode preparation.— Pt/C (50% mass on Vulcan carbon, E-Tek) or Ag/C (60% mass on Vulcan carbon, E-Tek) were used as electrode catalysts. A 30:1 ratio of catalyst to Nafion (catalyst binder) was used such that catalyst inks were prepared by mixing a total of 8.0 mg of Pt/C or 27 mg of Ag/C and 6.13 μL or 20.4 μL of 5 wt% Nafion solution (DuPont), respectively.[28,30] Here, Nafion acts as a relatively hydrophilic binder that facilitates catalyst wetting, as the liquid electrolyte is the primary source of ions. 200 μL of DI water and 200 μL of isopropyl alcohol were added as carrier solvents. The catalyst inks were sonicated (Branson 3510) for 1 hr to obtain a uniform mixture, which was then hand-painted onto 4 cm^2 of the hydrophobized carbon side of a carbon paper gas diffusion layer (35 BC, SGL carbon group) to create a gas diffusion electrode (GDE). For the microfluidic H_2/O_2 fuel cell, the final catalyst loading was 2 mg/cm^2 of Pt/C (50% mass Pt, 1 mg/cm^2 of Pt) for the anode and 2 mg/cm^2 of Pt/C (50% mass Pt, 1 mg/cm^2 of Pt) or 6.7 mg/cm^2 of Ag/C (60% mass Ag, 4 mg/cm^2 of Ag) for the cathode.

Fuel cell assembly and testing.— To assemble the fuel cell, shown in Figure 1, the cathode (Pt/C or Ag/C) and the anode (Pt/C) were placed on the opposite sides of a 0.1-cm or 0.2-cm thick polymethylmethacrylate (PMMA) window, such that the catalyst-coated GDE sides face the 3-cm long and 0.33-cm wide window machined in PMMA.[28] The microfluidic chamber volume was 0.1 or 0.2 mL. The window has one inlet and one outlet from the side for the electrolyte flow, aqueous solutions of potassium hydroxide (KOH, Sigma-Aldrich, 85 %, balance of H_2O) or sulfuric acid (H_2SO_4, Mallinckrodt, 95–98%, balance of H_2O). Two 1-mm thick graphite windows were used as current collectors. Polycarbonate gas flow chambers (5 cm (L) × 1 cm (W) × 0.5 cm (H)) were used to introduce both hydrogen and oxygen gases (laboratory grade, S.J. Smith), at 10 sccm each. The multilayer assemblies were held together with binder clips (Highmark). Fuel cell testing was conducted using a potentiostat (Autolab PGSTA-30, EcoChemie) at room temperature. For all studies, electrolyte flow rate was maintained at 0.3 mL min^{-1} using a syringe pump (2000 PHD, Harvard Apparatus).[6] Prior to experiments using the Ag cathode, the fuel cell was operated at 0.3 V for 20 min to activate the Ag catalyst; this procedure reduces Ag_2O formed on the cathode by holding it below the open-circuit voltage at which Ag^+ is favored over metallic Ag.[33,34] Fuel cell polarization curves were obtained by measuring steady-state currents at different cell potentials using General Purpose Electrochemical System (GPES) software (EcoChemie). The exposed geometric surface area of the electrode (1 cm^2) was used to calculate the current and power densities. A reference electrode (Ag/AgCl in saturated NaCl, BASi) was placed at the outlet of the electrolyte stream to allow for the independent analysis of polarization losses on the cathode and the anode.[35] The reference electrode was fitted with a polyethylene frit (Princeton Applied Research) in place of the original Vycor frit to prevent corrosion and contamination in alkaline media. After each experiment, the fuel cell was disassembled, the electrodes were rinsed with deionized water, and then the electrodes were dried under a laboratory fume hood.

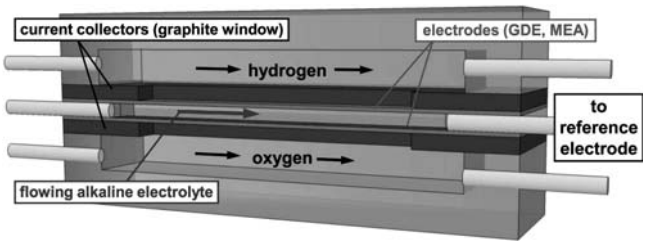

Figure 1. Diagram of the microfluidic fuel cell with a flowing electrolyte used in this study.

Impedance spectroscopy.— Electrochemical impedance spectroscopy (EIS) measurements were performed on the fuel cell using a Frequency Response Analyzer (FRA) module controlled by a potentiostat (Autolab PGSTAT-30, EcoChemie). The spectra were recorded in constant voltage mode by decreasing frequencies from 10 kHz to 30 MHz at 9 points/decade. The modulating voltage was 10 mV root mean squared. The high frequency x-axis intercepts represent the internal cell resistance (R_{cell}) which includes both electrolyte solution resistance and cell contact resistances. The diameter of the typical medium-frequency semicircular feature represents the charge-transfer resistance (R_{ct}) associated with the faradaic processes on the fuel cell electrodes. The low-frequency features represent the effects of mass transport limitations on fuel cell processes.[36]

Conductivity measurements.— The room temperature conductivity of electrolyte solutions was measured with an Orion 4 star pH/conductivity meter (Thermo Scientific) using a two-electrode conductivity cell (Duraprobe 018020MD). Before measurement, the conductivity cell was triple rinsed with deionized water and calibrated with a 1 M KCl solution with conductivity 111.9 mS cm^{-1}. Conductivity measurements were taken in triplicate and the average of the three values was used for the IR-corrections.

Results and Discussion

Single-electrode performance quantification.— First, we applied the analytical method by tracking individual electrodes simultaneously using a reference electrode, which yields the potential

of each electrode. Each electrode potential is plotted as overpotential. The overpotential is defined versus the equilibrium potential for the reaction. Equilibrium potentials under alkaline conditions, at pH 14, are −0.83 V vs. RHE for the anode and 0.4 V vs. RHE for the cathode, and are then shifted by −59 mV per increase of one pH unit.[1,8] A potential increase for the anode or a potential decrease for the cathode is considered to be positive overpotential which is thus associated with a decrease in the voltage of the fuel cell. These single-electrode overpotential plots display the qualitative kinetic, ohmic, and mass transport regions found on a regular, overall fuel cell IV curve. Figure 2 shows sample single-electrode plots for Pt electrodes tested in a microfluidic fuel cell (Figure 1) and operated with a 1 M KOH electrolyte, which roughly corresponds with the concentration of anions in an alkaline membrane. The kinetic losses shown in the polarization curve primarily come from the cathode, while the mass transport losses are due to the anode. As a result, the overpotential losses for the anode actually exceed the losses from the cathode for these two electrodes at high current densities, where mass transport losses become significant. In acidic media, particularly for a PEM fuel cell, the overpotential losses for the anode are insignificant due to the very fast kinetics[1] and any losses are typically attributed to the cathode. However, for alkaline media, these results demonstrate that hydrogen oxidation cannot be neglected in full cell analysis, and are supported by research with RDEs and in AEM fuel cells,[10,21] along with our previous research.[7,37]

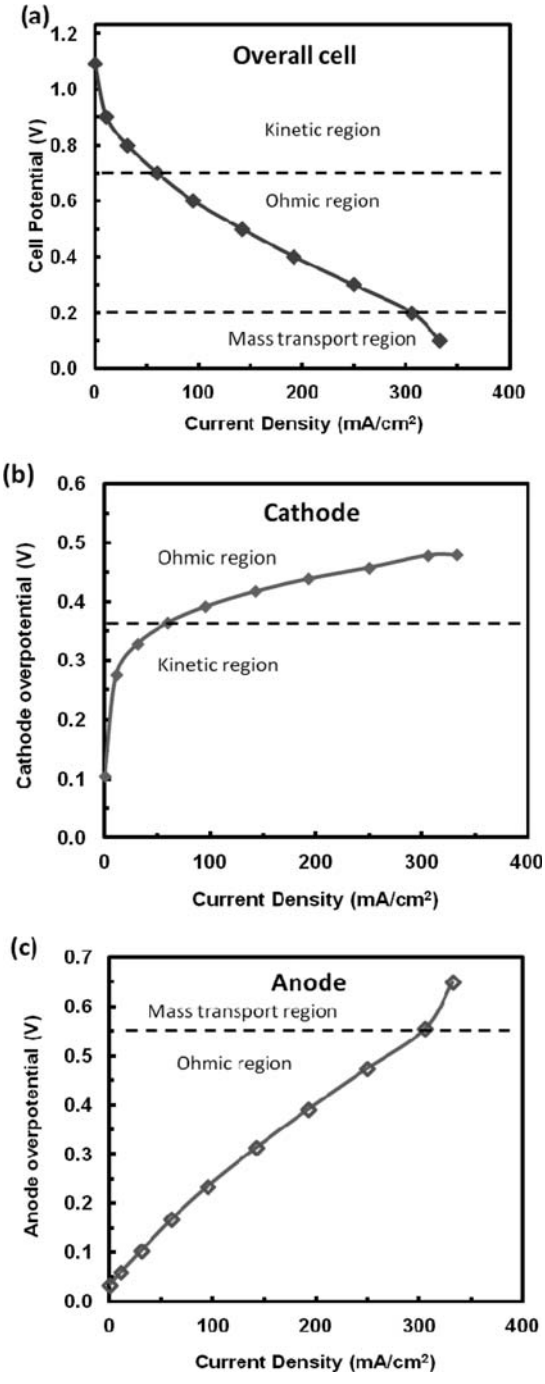

Figure 2. (a) Polarization curve and (b-c) single-electrode plots for a Pt/Pt alkaline fuel cell. Solid data points are used for the cathode while hollow points are used for the anode. Electrolyte: 1 M KOH. Electrolyte flow rate: 0.3 mL/min. H_2/O_2 feeds: 10 SCCM. At room temperature.

Quantitative data can be extracted from these plots to isolate behavior within a cell. This data is based on Equation 1, which is a linear approximation for the electrode overpotential as a function of R_{ohmic}, $\eta_{kinetic}$, and I:

$$\Delta V = R_{ohmic} I + \eta_{kinetic} \quad [1]$$

Where ΔV = electrode overpotential (V), R_{ohmic} = ohmic resistance (Ω-cm^2), I = current supplied by cell (mA/cm^2), $\eta_{kinetic}$ = voltage loss due to kinetics (V).

To find R_{ohmic} and $\eta_{kinetic}$, a linear fit, applied in the ohmic region, will produce the slope R_{ohmic} and the intercept $\eta_{kinetic}$ by minimizing the sum of the R^2 values for varying parameter values using the points in range. R_{ohmic} contains information about the electrolyte and electrode resistances, along with the mass transport losses; the R_{ohmic} parameter is not exclusively based on electrical resistance, but rather is the apparent resistance in the ohmic region. $\eta_{kinetic}$ contains information about kinetic/activation losses. Together, the absolute and relative values of these parameters yield detailed information about the causes and effects of fuel cell behavior that goes beyond the information that can garnered from typical polarization curves, impedance measurements, or two-electrode plots. In the following sections, we will demonstrate the utility of the single-electrode method introduced here by applying it to several comparative fuel cell studies of mass transport, ohmic, and kinetic phenomena.

Effect of electrode backing on mass transport.— Fuel cell electrodes use a variety of porous backing layers to facilitate gas transport while maintaining electrode structure. Two commonly used backings are carbon paper (a brittle and highly porous backing) and carbon cloth (a more robust but less porous backing layer). Varying the backing layer alters mass transport through the electrode, but does not significantly alter ohmic resistances or kinetic losses, since they are both carbon-based. To determine the effect of these backing layers, we tested two 2 mg/cm^2 Pt/C cathodes with 50 SCCM flowrates of O_2. The results are shown in Figure 3.

The resulting power density curves in Figure 3a show that use of the carbon paper cathode instead of the carbon cloth cathode increases power density by 14%. Although the polarization curves are mass transport-limited at current densities exceeding ∼300 mA/cm^2, these losses are due to transport issues on the anode (Figure 3c), while the cathodes remain in the ohmic region for tested current densities above 100 mA/cm^2 (Figure 3b). At high current density, the single-electrode plot for the cathodes actually exhibits decreasing electrode overpotential. This behavior is an artifact of the mass transport losses on the anode, and may be due to the reduced hydrogen crossover when the anode is starved of hydrogen. This behavior was apparent in a graph reported previously by others in a study on a membrane-based fuel cell with a reference electrode.[26] The backwards polarization in Figure 4c for the last two points on the anode overpotential curve for the carbon cloth is reproducible and was maintained for both forward and backward polarization with different Pt/C electrodes. Both single-electrode cathode curves start with identical losses at low current densities, but the carbon paper cathode increasingly outperforms the carbon cloth cathode as current densities increase. This behavior demonstrates that the two backing layers yield the same kinetic performance, but

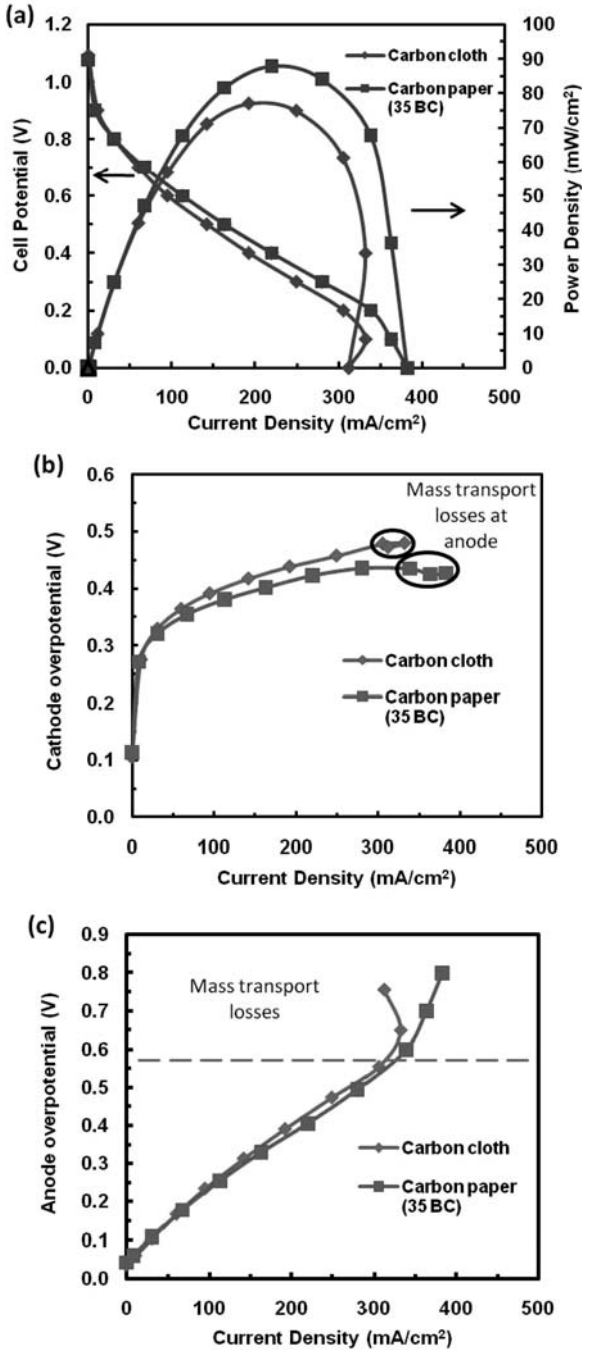

Figure 3. (a) Polarization and power density curves, (b) cathode plot, and (c) anode plot for a Pt/Pt alkaline fuel cell. Electrolyte: 1 M KOH. Electrolyte flow rate: 0.3 mL/min. H_2/O_2 feeds: 50 SCCM. At room temperature.

the mass transport losses are smaller for the carbon paper cathode. Table I shows that switching from carbon cloth to carbon paper decreases R_{ohmic} by 47%, indicating smaller mass transport losses for the carbon paper. However, $\eta_{kinetic}$ remains approximately constant, illustrating that the choice of backing layer does not alter the kinetic activity of the electrodes.

IR-correction of single-electrode plots.— IR-correction is a common method to remove the effect of ohmic resistance within an operating fuel cell from polarization data for analytical purposes.[17] Polarization curves are typically IR-corrected by adding the current times the electrolyte resistance, which is calculated from the electrolyte thickness and the conductivity of the electrolyte, to the polarization curve. Alternatively, some authors apply IR_{cell} corrections, where the R_{cell} value from EIS is assumed to be exclusively the full value of the electrolyte resistance, in the same fashion. IR_{cell} corrections frequently remove more of the ohmic losses from the cell, which can be used to better isolate kinetic losses but may neglect resistive losses, such as those between the electrode and the membrane, which are inherent to a given cell design.

Table I. Cathode fits for varying backing layer.

Backing	$\eta_{kinetic}$ (V)	R_{ohmic} (kΩ)
Carbon cloth	0.35	0.40
Carbon paper	0.36	0.21
Difference:	+3%	−47%

We tested the effect of altered ohmic resistance by testing our fuel cell with an electrode-to-electrode distance of either 2 mm or 1 mm. A thinner electrode separator would be expected to decrease the ohmic resistance and increase fuel crossover, but fuel crossover in hydrogen fuel cells typically has only a very minor effect. A 3 M KOH electrolyte was used here to attain higher current densities than would be possible with 1 M KOH.[37]

Figure 4a shows that decreasing the separator thickness from 2 mm to 1 mm results in an increase of the fuel cell power density by 31%, demonstrating that ohmic resistances indeed can significantly limit fuel cell performance despite the high conductivity of 509 mS/cm for the 3 M KOH electrolyte used. Without the limitations of ohmic resistance, the power density could be as high as 321 mW/cm^2, instead of the 206 mW/cm^2 actually produced; this number is obtained by multiplying the IR-corrected cell voltage by the current density at the point of maximum power density. The IR-corrected cell polarization curves fully overlap (Figure 4b), demonstrating that IR-correction accounts for all of the change in ohmic resistance. IR-corrected polarization curves thus simplify identification of kinetic and mass transport limitations as well as comparison of results between two different fuel cell setups by eliminating the effects of solution resistance. Analogous work by Lee et al. using a SOFC showed that the effect of decreased electrolyte thickness was largely ohmic, although the authors did not IR-correct their polarization curves.[38] The similar results from decreased electrolyte thickness in a different fuel cell setup illustrate the broader significance of IR-correction as applied to the microfluidic fuel cell.

The R_{ohmic} and $\eta_{kinetic}$ values obtained from the single-electrode plots for this data, shown in Table II, do have slightly varying values for R_{ohmic} based on the current range used for the fit. While our 2 mm data has a maximum current density of less than 550 mA/cm^2, the 1 mm data goes to 900 mA/cm^2 even after eliminating all points that showed minor mass transport effects (Figure 5). Here, we seek to determine the effects of current range on the fitted parameters, to determine if this method can be applied to data with substantially different current ranges. Using the method proposed here, we fit the data to obtain R_{ohmic} and $\eta_{kinetic}$. The 1 mm data was fitted for both the range of 150–550 mA/cm^2 and the range of 150–900 mA/cm^2. The results are shown in Table II.

The data shown in Table II demonstrates that the current range used for the fit can have a significant effect on the results. When both sets of data are fitted in the same current range, there is excellent agreement between the $\eta_{kinetic}$ values, showing that R_{ohmic} is the only source of differing values. As a result, all of the single-electrode fits shown in this paper are for identical current ranges, within a given section. Comparisons between data from different current ranges are not as reliable when using this method. This deviation arises from the kinetic behavior of the electrodes; this method approximates the kinetic overpotential as a constant value, when there is a logarithmic dependence of potential on current due to the Tafel equation.[17] Adding

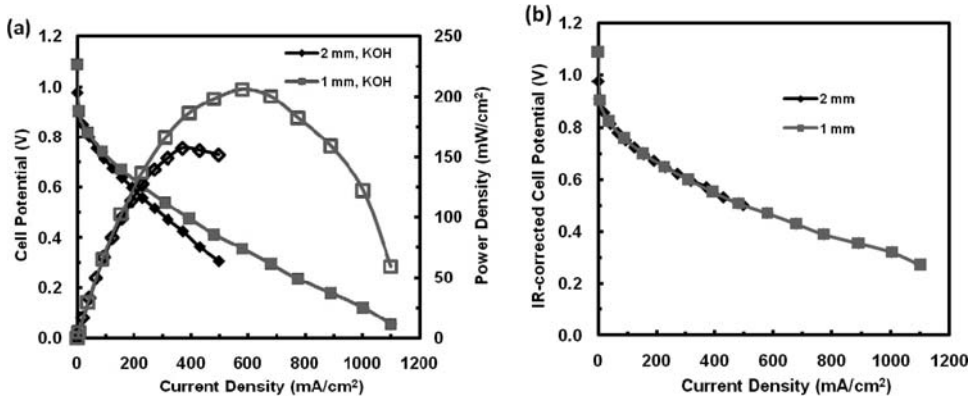

Figure 4. (a) Polarization curve and (b) IR-corrected polarization curve for a Pt/Pt alkaline fuel cell. Electrolyte: 3 M KOH. Electrolyte flow rate: 0.3 mL/min. H_2/O_2 feeds: 50 SCCM. At room temperature.

Table II. Quantitative fits for varying separator thickness.

Trial	Cathode $\eta_{kinetic}$ (V)	Cathode R_{ohmic} (Ω-cm^2)	Anode $\eta_{kinetic}$ (V)	Anode R_{ohmic} (Ω-cm^2)
2 mm (150–550 mA/cm^2)	0.35	0.46	0.09	0.53
1 mm (150–550 mA/cm^2)	0.36	0.37	0.09	0.42
1 mm (150–900 mA/cm^2)	0.37	0.32	0.11	0.35

a kinetic logarithmic term to the fit is beyond the scope of this paper, but could be a valuable direction for future work.

The next step for our research was to IR-correct our single-electrode polarization curves. While IR-corrected polarization curves are valuable, IR correction has not been used for two-electrode plots or single-electrode plots, because the IR-drop must be split between the two electrodes. A 50% split of the ohmic resistance between the two electrodes did not produce overlaying single-electrode plots, but the experimental values were fitted with 60% of the ohmic resistance at the anode. This minor difference may occur because OH^- anions are consumed at the anode surface, leading to higher local resistance. The single-electrode plots, shown in Figure 5, demonstrate a successful use of IR-corrections, since both of the plots overlay. In addition, the quantitative IR-corrected values differ by at most 3 mV or 7 Ω-cm^2 for $\eta_{kinetic}$ and R_{ohmic}, respectively. This result further supports our conclusion that the effect of varied separator thickness is purely ohmic for these conditions. *Thus, IR-correction of single electrode plots successfully isolates mass transport and kinetic effects for an individual electrode*.

Comparison between acidic and alkaline media.— To compare performance in alkaline media to the more common acidic media, we operated the fuel cell with 3 M KOH and with 3.5 M H_2SO_4. The concentration of sulfuric acid was chosen for the high conductivity of 660 mS/cm and the relatively high proton concentration, while higher concentrations were avoided due to potential sulfate poisoning. Both electrodes had a loading of 2 mg Pt/C/cm^2; the same electrodes were used in both alkaline and acidic media. The electrode used as the anode in alkaline media was used as the cathode in acidic media, to account for the shift in water generation from the anode to the cathode. The fuel cell used a 1 mm separator for these trials. The results from the trial are shown in Figures 6a–6c:

The resulting power density curves show that acidic media yields 82% higher power density than alkaline media. The improvement in performance is due to the greatly improved anode performance in acidic media (Figure 6c), which is supported by RDE experiments conducted by Sheng et al.[10] While the cathode yields superior performance in alkaline media (Figure 6b), the improved performance is not sufficient to offset the decreased anode performance. The better overall performance using acidic media is also influenced by the Nafion binder conducting protons in acidic media. While the usage of Nafion does favor acidic media over alkaline media, the equivalent alkaline binders have not been tested nearly as extensively as Nafion and often require very different preparation procedures (i.e., higher temperature

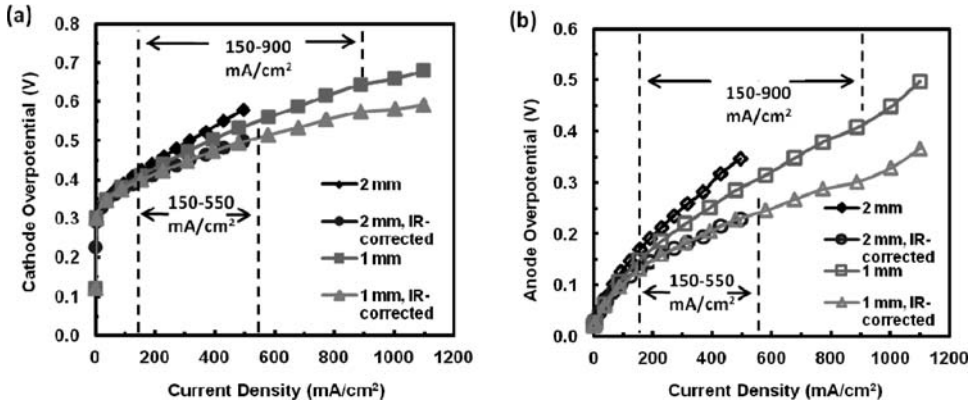

Figure 5. Single-electrode plots for (a) the cathode and (b) the anode in a Pt/Pt fuel cell. Electrolyte: 3 M KOH. Electrolyte flow rate: 0.3 mL/min. H_2/O_2 feeds: 50 SCCM. At room temperature.

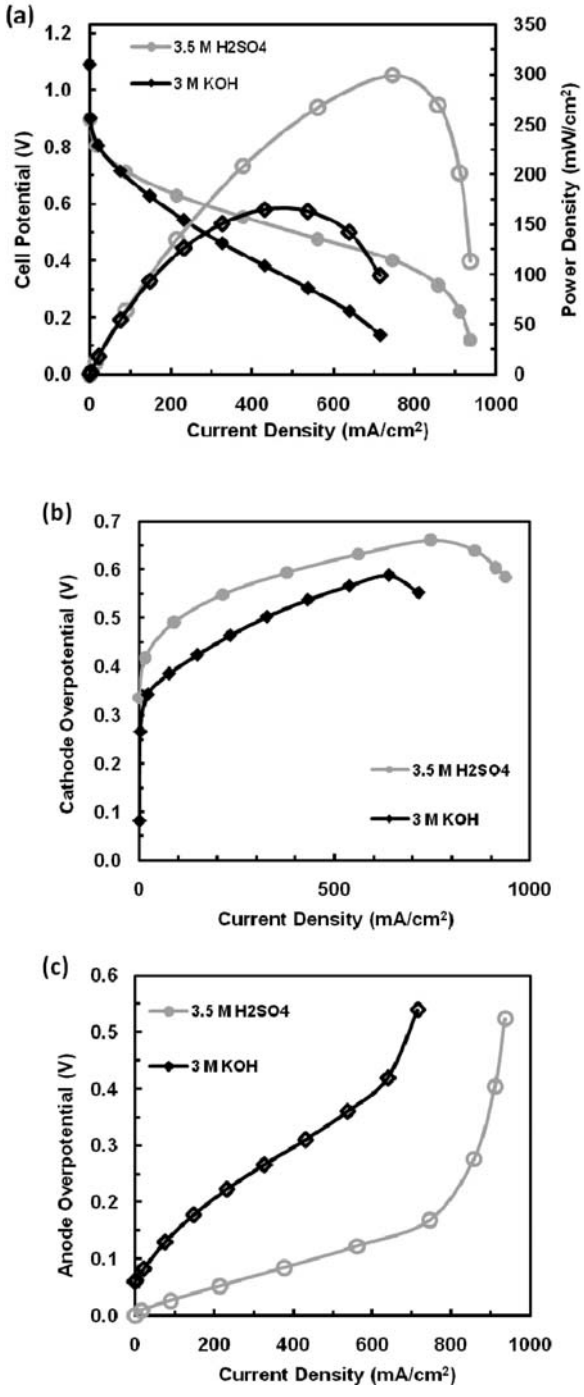

Figure 6. (a) Polarization and power density curves, (b) cathode plot, and (c) anode plot for a Pt/Pt fuel cell. Electrolyte flow rate: 0.3 mL/min. H_2/O_2 feeds: 10 SCCM. At room temperature.

or a different solvent). Since the power densities from alkaline media shown here are higher than previously reported alkaline media power densities of 110 mW/cm^2 in this setup,[6,7,30] the use of Nafion instead of the previous PTFE binder does not appear to inhibit performance.

The overall polarization curve in Figure 6a shows mass transport limitations for both setups, but the onset of mass transport limits occurs earlier in 3 M KOH. In both setups, the mass transport limitations occur at the anode. Since the anode in acidic media is not susceptible to flooding, due to the water consumption from the anodic hydrogen oxidation, the mass transport loss is due to the adsorption from

Table III. Single-electrode fits for acidic and alkaline media.

	Cathode		Anode	
Electrolyte	$\eta_{kinetic}$ (V)	R_{ohmic} (Ω-cm^2)	$\eta_{kinetic}$ (V)	R_{ohmic} (Ω-cm^2)
3.5 M H_2SO_4	0.50	0.24	0.01	0.20
3 M KOH	0.38	0.37	0.11	0.46

the HSO_4^- anions found in the electrolyte.[28,39] This specific result differs from conditions found inside PEMFCs, since there are not normally spectator anions within a PEMFC, but the other results can be considered broadly applicable to membrane-based setups.

Table III shows R_{ohmic} and $\eta_{kinetic}$ for acidic and alkaline media. The cathode $\eta_{kinetic}$ is 0.12 V less in alkaline media, demonstrating the improved ORR kinetics in alkaline media. However, the anode $\eta_{kinetic}$ increases by 100 mV and the anode R_{ohmic} increases by 130%, demonstrating the effects of inferior anode performance in alkaline media due to slower kinetics and water buildup.

Comparison with impedance in alkaline media.— The alkaline results from the single-electrode plots in the previous section were compared with results obtained using EIS. The impedance for the cell was determined at applied voltages of 800, 600, 400, and 300 mV. These voltages were used instead of compensating for the contact resistance in order to enable better comparisons with the values obtained for R_{ohmic} and $\eta_{kinetic,}$ since those values were obtained at applied voltages ranging from 800 mV to 0 mV in steps of 100 mV. The contact resistance ($R_{contact}$) at each applied voltage was calculated using the data from the polarization curves in Equation 2:

$$R_{contact} = (V - V_{applied})/I \quad [2]$$

Where V = voltage within the cell (V), $V_{applied}$ = voltage applied by potentiostat (V).

This $R_{contact}$ value was subtracted from the reported R_{cell} value to obtain the "corrected R_{cell}" value, which is the R_{cell} value that would be obtained in a real cell without the contact resistances inherent to our modular experimental cell.

For alkaline media, the impedance data shown in Figure 7a shows constant R_{cell} and reduced R_{ct} with decreasing voltage, following the trends established in our previous work.[6,37] The improved kinetic performance at lower voltages is responsible for the reduced R_{ct}.

The residual R_{cell}, which is the corrected R_{cell} subtracted by the known electrolyte ohmic losses, is shown in Table IV, along with the R_{CT} values. The residual R_{cell} encapsulates the losses from the electrodes themselves, due to the resistance between the catalyst and the backing layer, the resistance of the backing layer, and the resistance between the backing layer and the graphite current collector. The results show that the IR drop from the solution does not explain all of the resistance within our cell and electrode resistances play a significant role in determining performance. Comparing the sum of the cathode and anode R_{ohmic} values to the corrected R_{cell} values indicates that R_{ohmic} takes more than just the ohmic losses into account, as explained previously. As the cell voltage drops, the sum of R_{cell} and R_{CT} drops until it is similar to the total R_{ohmic} value, showing that determination of R_{ohmic} can yield similar results to impedance data without requiring additional experimentation.

Comparison with impedance in acidic media.— For acidic media, the impedance data in Figure 7b shows a much higher initial R_{CT} than in alkaline media at 0.8 V, due to the inferior acidic cathode kinetics; however, the acidic R_{CT} is lower than the alkaline R_{CT} at voltages 0.6 V and below, due to the superior acidic anode kinetics. The Nafion binder plays a role in reducing the acidic R_{CT} due to the proton conductivity.

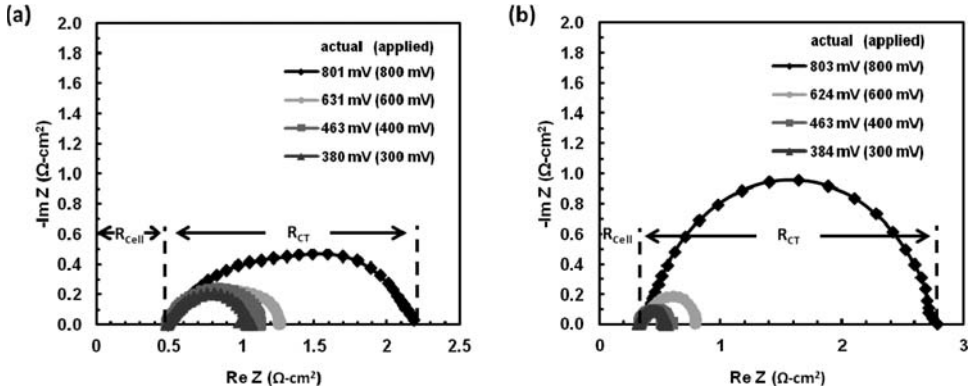

Figure 7. Impedance spectra for (a) alkaline media using 3 M KOH and (b) acidic media using 3.5 M H_2SO_4. Electrolyte flow rate: 0.3 mL/min. H_2/O_2 feeds: 10 SCCM. At room temperature.

Table V shows the R_{cell} and R_{CT} values for acidic media. The remaining R_{cell} for acidic media is smaller than that for alkaline media. This result is unexpected because the same electrodes were used in both trials. This result may indicate that the type of electrolyte, which is more conductive in acidic media, can play a role in the electrode resistance, since current must travel from the catalyst to the electrode and the binder is not as electrically conductive as the electrolyte. The total R_{ohmic} follows the same pattern as the residual R_{cell}, in that it is lower in acidic media. As the cell moves toward lower voltages, the combined R_{cell} and R_{CT} again become very similar to the total R_{ohmic}.

Comparison of acidic and alkaline conditions demonstrates one limitation of impedance. Although the R_{cell} and R_{ct} values for the acidic fuel cell at 600 mV applied are smaller than the values for the alkaline fuel cell at 300 or 400 mV applied, which would normally indicate superior performance from the fuel cell, the power density for the acidic fuel cell at 600 mV applied is smaller than the power density for the alkaline fuel cell at 300 or 400 mV applied. This result illustrates the limitations of impedance, in that lower resistances do not always correlate with superior power densities when comparing between different cells. Thus, standard EIS measurement in a fuel cell is restricted to functioning as an analytical method to explain differences in performance, whereas *quantification with single-electrode plots can predict differences in performance because it takes into account the electrode behavior that determines power density*.

Prediction of fuel cell power density using single-electrode data.— Since fuel cell electrodes are commonly tested under varying conditions with different anodes and cathodes, simulation of fuel cell performance with two electrodes together is desirable. Based on the information provided by single-electrode plots, it is trivial to simulate full cell performance with two electrodes that have been tested separately, if they are both tested under the same conditions. Equation 3 gives the cell voltage as a function of electrode overpotentials:

$$V = 1.23 - \Delta V_{cathode} - \Delta V_{anode} \quad [3]$$

The ΔV for each electrode is determined using Equation 1, yielding the cell voltage as a function of current (or vice versa). Finally, the power density (VI) can be calculated and plotted. The two electrode plots versus RHE can be created in the same fashion. The anode potential is identical to the overpotential and the cathode potential for a H_2 fuel cell follows Equation 4:

$$V_{cathode} = 1.23 - \Delta V_{cathode} \quad [4]$$

This method was used for a Ag cathode with $\eta_{kinetic} = 0.48$ V and $R_{ohmic} = 0.78\ \Omega\text{-cm}^2$, along with a Pt anode with $\eta_{kinetic} = 0.029$ V and $R_{ohmic} = 2.56\ \Omega\text{-cm}^2$. The fuel cell had a 2 mm thick electrolyte. The model and experimental power density curves and two electrode plots are shown in Figures 8a–8b.

As expected, the model shows good agreement with the experimental data, since electrode behavior is largely independent of the

Table IV. Impedance values for alkaline media.

Actual (Applied) voltage (mV)	Corrected R_{cell} (Ω-cm^2)	$R_{solution}$ (Ω-cm^2)	Remaining R_{cell} (Ω-cm^2)	R_{CT} (Ω-cm^2)	$R_{cell} + R_{CT}$ (Ω-cm^2)	total R_{ohmic} (Ω-cm^2)
801 (800)	0.26	0.20	0.06	1.65	1.91	0.83
631 (600)	0.30	0.20	0.10	0.78	1.08	0.83
463 (400)	0.30	0.20	0.10	0.62	0.92	0.83
380 (300)	0.29	0.20	0.09	0.56	0.85	0.83

Table V. Impedance values for acidic media.

Actual (Applied) voltage (mV)	Corrected R_{cell} (Ω-cm^2)	$R_{solution}$ (Ω-cm^2)	Remaining R_{cell} (Ω-cm^2)	R_{CT} (Ω-cm^2)	$R_{cell} + R_{CT}$ (Ω-cm^2)	total R_{ohmic} (Ω-cm^2)
803 mV (800 mV)	0.15	0.15	0.00	2.40	2.56	0.44
624 mV (600 mV)	0.20	0.15	0.05	0.45	0.65	0.44
463 mV (400 mV)	0.19	0.15	0.04	0.23	0.43	0.44
384 mV (300 mV)	0.18	0.15	0.03	0.23	0.41	0.44

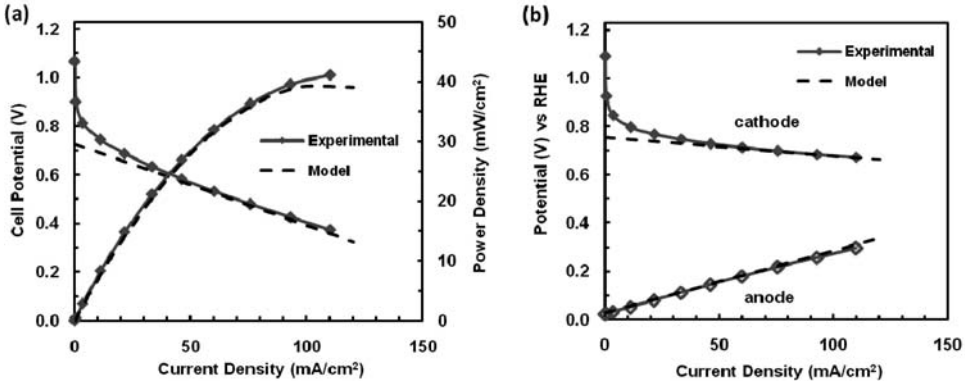

Figure 8. (a) Polarization curves and (b) two electrode plots for a Pt/Ag alkaline fuel cell. Electrolyte: 1 M KOH. Electrolyte flow rate: 0.6 mL/min. H_2/O_2 feeds: 50 SCCM. At room temperature.

other electrode (with exceptions for mass transport effects), as long as the other electrode still supplies the same reactive ions. The inaccuracy at low current density is expected because the kinetic losses are assumed to happen all at once, instead of increasing with current density. The power density of the cell is predicted to within 5% of the actual value, which can be considered a rough measure of the inaccuracy inherent to using a linear approximation for a section of a nonlinear curve. *However, the true value of this type of modeling stems from the ability to predict electrode behavior in new situations.* To test the predictive ability of this method, we chose to test the Ag electrode under new conditions with 3 M KOH instead of 1 M KOH, a 1 mm thick electrolyte instead of a 2 mm electrolyte, and an anode that can achieve higher current densities. To obtain the effects of using 3 M KOH instead of 1 M KOH, we tested a Ag electrode that used a different backing layer; R_{ohmic} decreased by 25 Ω-cm^2 and $\eta_{kinetic}$ decreased by 24 mV when changing to 3 M KOH. For the effect of changing electrolyte thickness to 1 mm, we used the method stated in the previous section to IR-correct using half of the 2 mm solution resistance. Even though IR-corrections were tested for a Pt cathode instead of a Ag cathode, the effect of the electrolyte, along with the OH^- gradient, would not significantly change as a function of the catalyst. The flow rate was also halved to maintain the same superficial velocity through the channel. The model and experimental power density curves and two electrode plots are shown in Figures 9a–9b.

The power density prediction was accurate within 10% inside the model range, with deviation exceeding 30% at current densities below 9 mA/cm^2 or above 500 mA/cm^2. The deviation at high current densities occurs because the additional kinetic losses are smaller. The main inaccuracy comes from the anode at higher current densities, possibly due to the same reason. Further testing could yield better approximations for the expected losses at higher current densities.

The next question would be whether these results obtained with a microfluidic fuel cell are scalable to larger-scale fuel cells, such as membrane-based fuel cells in a stack. While there may be differences in the magnitude of changes due to the differences in each setup, the overall principles remain the same, so the methodology could potentially work with results obtained from, say, a membrane fuel cell with a specially designed reference electrode.[16,20,21]

Conclusions

Here, we reported on our method to quantify single electrode plots and we apply this method with our experiments to quantifiably determine the effects of ohmic and mass transport losses using single-electrode plots, based on a reference electrode. We demonstrated that losses from both electrodes are substantial in an alkaline fuel cell, and that ohmic and mass transport losses are shown to only significantly affect R_{ohmic}. IR-corrections were used to isolate individual kinetic and mass transport losses at each electrode within our operating fuel cell. We determined that acidic media currently outperforms alkaline media with Nafion-bonded electrodes at lower potentials, due to the substantial anode losses in alkaline media. Single-electrode plots showed good agreement with impedance data while demonstrating a superior correlation with the electrode behavior that ultimately determines the power density of the cell. Finally, we demonstrated the ability of single-electrode plots to predict fuel cell behavior for electrodes tested in new conditions.

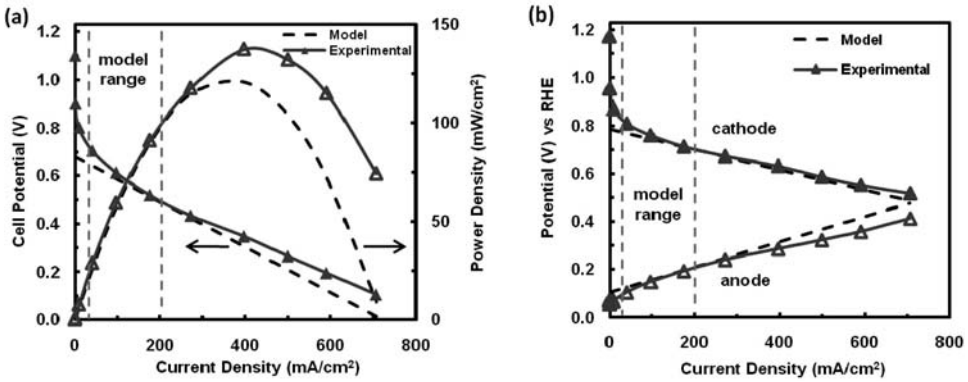

Figure 9. (a) Polarization curves and (b) two electrode plots for a Pt/Ag alkaline fuel cell. Electrolyte: 3 M KOH. Electrolyte flow rate: 0.3 mL/min. H_2/O_2 feeds: 50 SCCM. At room temperature.

Quantifiable usage of these single-electrode plots offers the potential to determine and predict electrode behavior in a wide variety of tested situations. By knowing the effects of an ohmic or mass transport change for a given set of electrodes, the next step would be to predict whole cell performance using different electrodes. Since ohmic and mass transport behavior are often similar for electrodes designed to catalyze the same reaction, fuel cell modeling based on empirical data could reduce the need to create a new fuel cell to test any change in a variable. This general methodology can be applicable to any type of fuel cell (i.e., PEM, AEM, solid oxide) that can use a reference electrode and thus analyzes going beyond the basic level of maximum power density analysis or impedance results are now possible.

Acknowledgments

We gratefully acknowledge financial support from the Army Research Office (Grant W911NF-10-2-0054), Department of Energy (DE-FG02005ER46260) and from the National Science Foundation (CAREER grant CTS 05-47617). The authors also thank Fikile R. Brushett for stimulating discussions.

References

1. L. Carrette, K. A. Friedrich, and U. Stimming, *Chemphyschem*, **1**, 162 (2000).
2. Z. Lu, X.-D. Zhou, J. Templeton, and J. W. Stevenson, *Journal of the Electrochemical Society*, **157**, B964 (2010).
3. K. J. Yoon, P. Zink, S. Gopalan, and U. B. Pal, *Journal of Power Sources*, **172**, 39 (2007).
4. H. M. Xiao, T. L. Reitz, and M. A. Rottmayer, *Journal of Power Sources*, **183**, 49 (2008).
5. G. F. McLean, T. Niet, S. Prince-Richard, and N. Djilali, *International Journal of Hydrogen Energy*, **27**, 507 (2002).
6. F. R. Brushett, W. P. Zhou, R. S. Jayashree, and P. J. A. Kenis, *Journal of the Electrochemical Society*, **156**, B565 (2009).
7. M. S. Naughton, F. R. Brushett, and P. J. A. Kenis, *Journal of Power Sources*, **196**, 1762 (2011).
8. J. S. Spendelow and A. Wieckowski, *Physical Chemistry Chemical Physics*, **9**, 2654 (2007).
9. Matthew S. Thorum, J. Yadav, and Andrew A. Gewirth, *Angewandte Chemie*, **121**, 171 (2009).
10. W. C. Sheng, H. A. Gasteiger, and Y. Shao-Horn, *Journal of the Electrochemical Society*, **157**, B1529 (2010).
11. A. R. Kucernak and E. Toyoda, *Electrochemistry Communications*, **10**, 1728 (2008).
12. F. R. Brushett, R. S. Jayashree, W. P. Zhou, and P. J. A. Kenis, *Electrochimica Acta*, **54**, 7099 (2009).
13. L. J. Bregoli, *Electrochimica Acta*, **23**, 489 (1978).
14. K. A. Striebel, F. R. McLarnon, and E. J. Cairns, *Journal of the Electrochemical Society*, **137**, 3360 (1990).
15. A. E. S. Sleightholme, J. R. Varcoe, and A. R. Kucernak, *Electrochemistry Communications*, **10**, 151 (2008).
16. S. Eccarius, T. Manurung, and C. Ziegler, *Journal of the Electrochemical Society*, **154**, B852 (2007).
17. A. J. Bard and L. R. Faulkner, *Electrochemical methods : fundamentals and applications / Allen J. Bard, Larry R. Faulkner*, Wiley, New York (1980).
18. J.-W. Kim, A. V. Virkar, K.-Z. Fung, K. Mehta, and S. C. Singhal, *Journal of the Electrochemical Society*, **146**, 69 (1999).
19. G. Li and P. G. Pickup, *Journal of the Electrochemical Society*, **150**, C745 (2003).
20. D. Gerteisen, *Journal of Applied Electrochemistry*, **37**, 1447 (2007).
21. R. Zeng, S. D. Poynton, J. P. Kizewski, R. C. T. Slade, and J. R. Varcoe, *Electrochemistry Communications*, **12**, 823 (2010).
22. M. Nagata, Y. Itoh, and H. Iwahara, *Solid State Ionics*, **67**, 215 (1994).
23. Z. Liu, J. S. Wainright, W. Huang, and R. F. Savinell, *Electrochimica Acta*, **49**, 923 (2004).
24. G. Li and P. G. Pickup, *Electrochemical and Solid-State Letters*, **9**, A249 (2006).
25. J. Rutman and I. Riess, *Electrochimica Acta*, **52**, 6073 (2007).
26. Y. Tsutsumi, S. Ono, and M. Eguchi, *Electrical Engineering in Japan*, **172**, 10 (2010).
27. P. Piela, T. E. Springer, J. Davey, and P. Zelenay, *Journal of Physical Chemistry C*, **111**, 6512 (2007).
28. R. S. Jayashree, M. Mitchell, D. Natarajan, L. J. Markoski, and P. J. A. Kenis, *Langmuir*, **23**, 6871 (2007).
29. F. R. Brushett, H. T. Duong, J. W. D. Ng, R. L. Behrens, A. Wieckowski, and P. J. A. Kenis, *Journal of the Electrochemical Society*, **157**, B837 (2010).
30. F. R. Brushett, M. S. Thorum, N. S. Lioutas, M. S. Naughton, C. Tornow, H. R. Jhong, A. A. Gewirth, and P. J. A. Kenis, *Journal of the American Chemical Society*, **132**, 12185 (2010).
31. A. Küver, I. Vogel, and W. Vielstich, *Journal of Power Sources*, **52**, 77 (1994).
32. G. J. Offer, P. Shearing, J. I. Golbert, D. J. L. Brett, A. Atkinson, and N. P. Brandon, *Electrochimica Acta*, **53**, 7614 (2008).
33. E. Gülzow and M. Schulze, *Journal of Power Sources*, **127**, 243 (2004).
34. M. Cifrain and K. V. Kordesch, *Journal of Power Sources*, **127**, 234 (2004).
35. E. R. Choban, P. Waszczuk, and P. J. A. Kenis, *Electrochemical and Solid-State Letters*, **8**, A348 (2005).
36. T. J. P. Freire and E. R. Gonzalez, *Journal of Electroanalytical Chemistry*, **503**, 57 (2001).
37. F. R. Brushett, M. S. Naughton, J. W. D. Ng, L. Yin, and P. J. A. Kenis, *International Journal of Hydrogen Energy*, **37**, 2559 (2011).
38. Y. Lee, J. H. Joo, and G. M. Choi, *Solid State Ionics*, **181**, 1702 (2010).
39. M. E. Gamboa-Aldeco, E. Herrero, P. S. Zelenay, and A. Wieckowski, *Journal of Electroanalytical Chemistry*, **348**, 451 (1993).